

Sensitivity analysis of sediment resuspension parameters in coastal area of southern Lake Michigan

Cheegwan Lee

Battelle Memorial Institute, Seattle Research Center, Seattle, Washington, USA

David J. Schwab and Nathan Hawley

NOAA Great Lakes Environmental Research Laboratory, Ann Arbor, Michigan, USA

Received 13 February 2004; revised 2 July 2004; accepted 1 December 2004; published 8 March 2005.

[1] Model sensitivity analysis was performed to identify and compare quantitatively the important resuspension parameters in the coastal area of southern Lake Michigan. A one-dimensional resuspension and bed model capable of dealing with the type of mixed sediments (fine-grained+sand) common in the coastal area was developed and utilized to compare with measured suspended sediment concentrations. The results show that the most sensitive parameters in the model are the fraction of fine-grained materials and sediment availability. Other resuspension parameters such as settling velocity, critical shear stress, and erosion rate constant are also found to be important and may cause up to a 40% difference in suspended sediment concentration. Among those, the absolute magnitude of settling velocity is most crucial in controlling the first order prediction.

Citation: Lee, C., D. J. Schwab, and N. Hawley (2005), Sensitivity analysis of sediment resuspension parameters in coastal area of southern Lake Michigan, *J. Geophys. Res.*, 110, C03004, doi:10.1029/2004JC002326.

1. Introduction

[2] Fine-grained sediments mixed with sands are common in coastal areas. Resuspension and transport of fine-grained sediments are often an important aspect of ecosystems in aquatic environments. For example, the amount of fine-grained sediment resuspended along the coastline of southern Lake Michigan can exceed the fluxes of external inputs from bluff erosion, and sediment redistribution along the eastern part of the lake is of great importance in the aquatic ecological system [Eadie *et al.*, 1984; Eadie and Robbins, 1987; Robbins and Eadie, 1991; Brooks and Edgington, 1994]. However, the resuspension of fine-grained sediment, especially when mixed with sand, is poorly understood in spite of several decades of research. A number of laboratory studies [Krone, 1962; Partheniades, 1965; Parchure and Mehta, 1985; Otsubo and Muraoka, 1988; Torfs, 1995; Lick and McNeil, 2001; Lee *et al.*, 2004] have improved our knowledge of the resuspension behavior of fine-grained materials. However, transferring the results of these laboratory experiments to field studies has been problematic because of the complexity of real sediments and of natural flows.

[3] Both numerical modeling studies and field measurements have been performed in Lake Michigan to study annually recurrent sediment resuspension events, often called "resuspension plume." An integrated hydrodynamic, wind-wave, and sediment transport model has been used to simulate episodic events [Beletsky *et al.*, 2000; Lou and Schwab, 2000]. The simulation results qualitatively

reproduced the plume but did not reproduce the recently measured deposition pattern [Eadie and Lozano, 1999; Robbins *et al.*, 2003] or the long-term sediment transport (average timescale of sediment transport from source to sink is several years). Field measurements in Lake Michigan have been conducted previously using tripods equipped with a current meter, a pressure gage, and a turbidity meter [Hawley and Lesht, 1995; Hawley and Lee, 1999]. These tripods have been deployed at many locations. The measurements show a distinct correlation between resuspension and bed shear stress (which is mainly due to wind waves), and that resuspension occurs frequently in shallow water (<30 m). However, common resuspension models [Krone, 1962; Partheniades, 1965; Parchure and Mehta, 1985] based on laboratory experiments usually depend on site-specific or event-specific calibration.

[4] Analysis of previous and current field measurements shows that suspended sediments are vertically well mixed and the concentration distributions are relatively uniform along and across the shore within the resuspension plume [Eadie *et al.*, 2002]. Calculations using a common resuspension model [Krone, 1962; Parchure and Mehta, 1985], where the resuspension rate is directly proportional to excess bottom shear stress, give an order of magnitude difference in resuspension flux across the plume if a constant resuspension coefficient is used. This raises a question: Why is the distribution of total suspended materials (TSM) relatively uniform across the resuspension plume despite an order of magnitude variation in bed stress? The main reason for the uniformity may be attributed to lateral mixing, to temporal and spatial variations of field resuspension parameters (fine-grain fraction and availability, critical shear stress for erosion and deposition, erosion rate

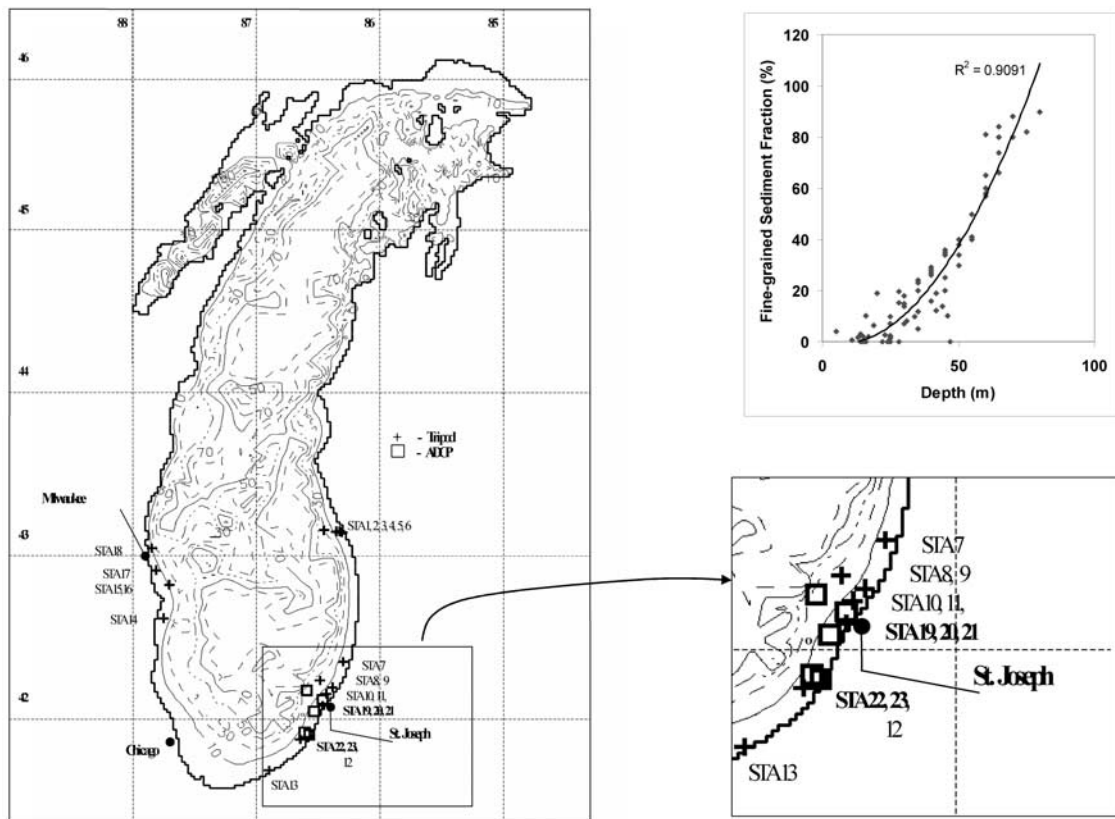


Figure 1. ADCP locations (open squares) and tripod locations (plus signs) in southern Lake Michigan. Contour lines show the percentage of fine-grained materials ($<60 \mu\text{m}$). Upper right graph shows the correlation between fine-grained materials and water depth.

constant, floc settling velocity) determined by the bed properties, or to uncertainty in estimation of the bed stress. However, satellite and in situ measurement data indicate that neither lateral mixing nor variations in critical shear stress are responsible. The sharp gradient of suspended sediment concentration at the edge of plume is clearly observed from satellite images and field data, indicating low lateral mixing. The critical shear stress of fine-grained materials in the top surface bed layer is relatively invariant in the coastal area with a range of $0.05\sim 0.15 \text{ Pa}$ [Hawley and Lesht, 1995; Hawley and Lee, 1999]. The spatial variations of erosion rate and floc settling velocity are probably not the reason, either. The error in bed stress estimation mainly originates from the estimation of friction coefficient over an inhomogeneous lake bottom, since the GLERL/Donelan wave model [Schwab *et al.*, 1984] can accurately predict wave parameters in Lake Michigan. As sediment transport models are usually calibrated with measurements, an improvement in estimating the absolute magnitude of bed stress may not be practically important. Although spatial and temporal variations of bed stress caused by bedforms interacting with flow may affect the distribution of suspended materials by modulating the turbulent flow regime, in the present study these effects are not considered to be important.

[5] Several studies [Van Niekert *et al.*, 1992; Harris and Wiberg, 2002; Harris *et al.*, 2003] suggest that the rate and gradient of suspended sediment flux depends on the

availability of suspendable sediment in the active bed layer. The sediment distribution in Lake Michigan is nonhomogeneous, and the fraction of fine-grained materials is fairly well correlated with water depth [Chambers and Eadie, 1980; Eadie and Lozano, 1999], showing an increasing percentage of fine-grained materials with increasing water depth (see Figure 1). Since the coastal area is a temporary repository where frequent resuspension occurs, fine sediments will be resuspended before permanent burial, and the fraction and availability can be connected to the resuspension frequency and intensity correlated to water depth. Therefore it is hypothesized that the fine-grained sediment fraction and availability limit the sediment resuspension in a way to make a relatively uniform plume.

[6] A common issue arising from both field and numerical modeling studies is identifying and quantitatively comparing the important resuspension parameters, in order to better understand how much they affect the suspended sediment concentration, and how much uncertainty is involved in numerical prediction. Better knowledge of this issue is going to improve the prediction by a sediment transport model. With this motivation, we hypothesized that the fine-grained sediment fraction and availability are controlling parameters of resuspension flux along with others mentioned above. Incorporating these parameters, a new resuspension model and recent field experiment data were used to investigate quantitatively the effects of

resuspension parameters on sediment resuspension within measurement uncertainties in southern Lake Michigan.

2. Sediment Dynamics and Bed Model

[7] A one-dimensional resuspension model capable of dealing with mixed sediments was developed to simulate time series of suspended sediment concentration locally resuspended by waves and currents. The model consisted of two parts: sediment dynamics model and bed model. The sediment dynamics model includes entrainment, deposition, and flocculated and nonflocculated settling of mixed sediments. The bed model calculates the modification of sediment texture in the sequentially specified bed layers. The two models were coupled to interact through entrainment and deposition processes in a way that conserves sediment mass. For a simplified analysis, the consolidation effect was not considered due to the small fraction of fine-grained materials (<6%) and to the confinement of fine-grained materials in the top surface layer. The critical shear stresses for fine-grained sediment and sand were separately specified or estimated by assuming no hiding and cohesion effects of interstitial fine-grained materials between sand particles.

[8] The depth-averaged sediment dynamics model is described as

$$h \frac{dC}{dt} = F_R - F_D + F_A + F_L, \quad (1)$$

where h is the water depth, C is the depth-averaged suspended sediment concentration, F_R is the resuspension flux, F_D is the deposition flux, F_A is the net advection flux, and F_L is the lateral flux from bluff erosion and tributaries. Therefore, C is totally controlled by the difference of F_R , F_D , F_A , and F_L by assuming small horizontal diffusion. The effect of F_A is not included in the numerical model. In an area of active resuspension, such as the plume along the eastern part of Lake Michigan, F_R and F_D are the main flux terms for the fine-grained sediment budget. Advection is small due to the relatively uniform concentration along the resuspension plume. The eastern shore is composed mainly of sand and does not provide a significant lateral flux of fine-grained material.

[9] In the current model, a common resuspension formulation was modified to consider the effect of sediment availability and the dependence of erosion rate on the remaining fine-grained fraction, f_{cs} . The total amount of fine-grained sediment erosion is limited by the available amount of fine-grained materials and the sands remaining in the surface bed layer. In sandy beds, winnowing of fine materials from the thin active layer can quickly result in bed armoring that reduces resuspension [Harris et al., 2003]. A simple linear dependence of erosion rate on f_{cs} is arguable, but few experiments exist. The net resuspension flux for the fine-grained sediment part can be written as

$$F_R - F_D = \sum_{i=1}^{n_c} (f_{f,i} f_{cs} M_0 (\tau_b - \tau_c) - w_{s,i} f(R, \sigma_d) C_i P_{D,i}) \quad (2)$$

$$P_{D,i} = \begin{cases} 1 - \tau_b / \tau_{cd,i} & \tau_b < \tau_{cd,i} \\ 0 & \tau_b > \tau_{cd,i} \end{cases},$$

where n_c is the number of floc size classes, $f_{f,i}$ is the fraction of each floc size class determined by the floc model (see equation (7)), f_{cs} is the fraction of fine-grained sediment in the bed, M_0 is the resuspension rate coefficient, τ_b is the bed shear stress, τ_c is the critical shear stress for resuspension (if $\tau_b < \tau_c$, $F_R = 0$), $\tau_{cd,i}$ is the critical shear stress for deposition of each size class, $w_{s,i}$ is the settling velocity of each sediment size class, $f(R, \sigma_d)$ is a function for converting the depth-averaged concentration to the concentration at the deposition level (σ_d) (see Appendix A), C_i is the depth-averaged suspended sediment concentration for each size class, and $P_{D,i}$ is the deposition probability function for each floc size. For sand, the net resuspension flux is calculated as follows:

$$F_R - F_D = \sum_{i=1}^{n_s} w_{s,i} f(R, \sigma_r) [f_{ns,i} C_{eq,i} - C_i], \quad (3)$$

where n_s is the number of sand size classes, σ_r is the reference height, $f_{ns,i}$ is the fraction of sand for each size class, and $C_{eq,i}$ is the depth-averaged equilibrium concentration for each size class which is estimated from the equilibrium reference concentration at $z = \sigma_r$. The equilibrium reference concentration was calculated by Smith and McLean's [1977] formula.

[10] The flocculation processes are parameterized to estimate size (d_f), fraction ($f_{f,i}$), and density (ρ_f) of sediment flocs at the deposition level (σ_d). Then the resulting settling velocity spectrum (w_s) is calculated using the estimated floc size and density. Assuming the commonly accepted log-normal distribution of floc size class [Lick and Lick, 1988], the probability density (PDF) and the cumulative density function (CDF) were developed to estimate the fraction and size distribution.

$$PDF(d_f) = \frac{1}{S d_f \sqrt{2\pi}} e^{-(\ln d_f - \ln d_{fm})^2 / (2S^2)} \quad (4)$$

$$CDF(d_f) = \frac{1}{2} \left[1 + \operatorname{erf} \left(\frac{\ln d_f - \ln d_{fm}}{S\sqrt{2}} \right) \right], \quad (5)$$

where S are the standard deviation of $\ln(d_f)$, erf is the error function, and d_{fm} is the median floc diameter. S was determined by fitting Lick and Lick's [1988] experimental results, and is estimated to be about 0.6. The median floc diameter (d_{fm}) is determined from the following experimentally based formula assuming a dynamic equilibrium of floc size distribution during the current modeling time step (1 hour) [Lick and Lick, 1988; Gailani et al., 1991]:

$$d_{fm} = \left(\frac{\alpha_0}{C_f G} \right)^{1/2}, \quad (6)$$

where $\alpha_0 = 10^{-8} \text{ g}^2/\text{cm}^3 \text{ s}^2$ is the experimentally determined constant for fine-grained sediments in freshwater [Ziegler and Nisbet, 1995], C_f is the fine-grained sediment concentration (g/cm^3), and G is the fluid shear stress (dyne/cm^2) at the reference level. The fraction of each floc size class ($f_{f,i}$) is calculated from the CDF as follows:

$$f_{f,i} = CDF(d_{f,i}) - CDF(d_{f,i-1}). \quad (7)$$

The average floc diameter (first moment of PDF) in the specified size ranges and the corresponding floc density [Lick and Lick, 1988] are approximated by

$$d_f = \int_{d_{f,i-1}}^{d_{f,i}} x \cdot PDF(x) dx / \int_{d_{f,i-1}}^{d_{f,i}} PDF(x) dx \quad (8)$$

$$\rho_f = \rho_w + 1.65 \left(\frac{4 \times 10^{-4}}{d_f} \right)^{0.8}, \quad (9)$$

where $d_{f,i-1}$ and $d_{f,i}$ are the lower and upper limit of specified size range, and x is the integration variable. This average floc diameter depends on fluid shear velocity and fine-grained sediment concentration as implied in equations (4) and (6).

[11] The resulting settling velocity of each sediment size class is estimated by

$$w_s = C_{FD} \frac{8\nu_m}{d_s} \left(\left[1 + 0.0139d_*^3 \right]^{0.5} - 1 \right), \quad (10)$$

$$d_* = d_s \left[\frac{(\rho_s/\rho_w - 1)g}{\nu_m^2} \right]^{1/3},$$

where w_s is the fall velocity; C_{FD} is the effective settling coefficient considering particle shape, pore space, and organic contents, $C_{FD} = 1$ for sand, $C_{FD} < 1$ for a plate-like floc; ν_m is the kinematic viscosity of a mixture (water and sediment); d_* is the nondimensional sediment diameter; d_s is the sediment diameter; ρ_s is the sediment density (2.65 g/cm^3 for sand and $d_s = d_f$, $\rho_s = \rho_f$ for floc), and ρ_w is the density of water (g/cm^3). A notable feature of the settling velocity formulation is that it does not use the common empirical formula (in the form of ad_{fm}^b) but a physically based formula. Originally, the formula (10) was developed to estimate the fall velocity of spherical sand particles under a wide range of Reynold numbers ($\text{Re}_p = w_s d / \nu$) but herein is modified to consider the lumped effects of plate-like shape, pore space, and organic content of a sediment floc by introducing the effective settling coefficient (C_{FD}). C_{FD} is set to 0.3 based on experimental data [Chakraborti and Atkinson, 2003].

[12] Deposition (F_D) and resuspension (F_R) terms become a source and sink term for the bed model. Sediment is added to or removed from the bed at the net exchange rate ($F_R - F_D$). A mass exchange rate is converted to/from a volumetric rate of change by the bulk density of bed.

$$\frac{\partial z_b}{\partial t} = -\frac{1}{\rho_b} (F_R - F_D), \quad (11)$$

where z_b is the top bed layer thickness, and ρ_b is the dry bed bulk density. Subscripts for each size class were omitted. The sediment bed is treated as a sequence of layers, below which is a nonerodible surface. Each layer has its own characteristics: thickness, sediment fraction, and bulk density. Net sediment deposits build up a surface layer whose thickness does not exceed an initially specified layer thickness. A new surface layer is formed when the total thickness of surface layer (net sediment deposit + old surface layer thickness) exceeds the initially specified value.

Net sediment erosion reduces the surface layer. When the mass of resuspended sediment exceeds the amount in the surface layer, the total resuspended mass is limited to that mass and then a new layer is exposed to eroding flow at next time step. To avoid erosion limitation due to a very thin surface layer remaining numerically during high flow, the bed model pushes up the bed sediment surface to maintain a certain thickness of surface layer, herein 3 mm. In this pushing process the bed characteristics are recalculated based on mass conservation. Consolidation effects are not considered in the present study case as the fine-grained sediment fraction is low and mostly confined to the top surface layer.

[13] The combined wave and current bed shear stress is calculated simply by the sum of a wave and current bed shear stress since the consideration of nonlinear interaction does not improve results in the present study.

$$\tau_{cw} = [\tau_{wm}^2 + \tau_c^2]^{1/2}, \quad (12)$$

where τ_{cw} is the combined shear stress, τ_{wm} is the maximum wave shear stress, and τ_c is the current shear stress. Jonsson [1966] defined

$$\tau_{wm} = \frac{1}{2} \rho f_w u_{wb}^2, \quad (13)$$

where f_w is the wave friction factor and u_{wb} is the maximum near-bottom wave velocity. Here f_w is calculated by the experimental relations in different flow regimes [Swart, 1974; Kamphuis, 1975; Justesen, 1988]. The current shear stress is calculated by a simple formula defined as

$$\tau_c = \frac{1}{2} \rho C_D U^2, \quad (14)$$

where C_D is the drag coefficient, herein 0.005, and U is the depth-averaged current velocity.

3. Results and Discussions

3.1. Field Data Collection and Analysis

[14] Five ADCP moorings were deployed during two different time periods at five locations along the coast in southern Lake Michigan (see Table 1 and Figure 1) as part of the Episodic Events-Great Lakes Experiment (EEGLE) project. At STA 19, 20, and 21, the ADCPs measured current profiles continuously at 2 Hz over 30 min burst and also the resuspended sediment concentration (inferred from acoustic backscattering signal). At STA 22 and 23, the ADCPs measured wave parameters, current profile, and suspended sediment concentration at 2 Hz over 20 min every hour. An OBS sensor was moored at the same height as the first ADCP bin (3.47 and 1.6 m for STA 22 and 23) to calibrate acoustic backscattering signals and measured turbidity at 0.1 Hz for 5 min every 20 min. Measurements from STA 19 and 20 were used to verify the new sediment dynamics model calibrated from the recent observations at STA 22 and 23.

[15] Back-scattering signal strength was converted from raw echo intensity using an equation proposed by Deines [1999], and was calibrated with the OBS data and averaged

Table 1. Description of Five ADCP Measurement Stations^a

Station Number	Latitude	Longitude	Depth, m	Silt+Clay, %	Period	Frequency
STA 19	42°05.99'N	86°33.53'W	20.5	6.3	26/08/98~07/07/99	300 KHz
STA 20	42°10.38'N	86°29.37'W	21.1	6.6	26/08/98~20/04/99	1200 KHz
STA 21	42°13.75'N	86°36.82'W	40.5	25.7	26/08/98~27/05/99	1200 KHz
STA 22	41°58.11'N	86°37.89'W	19.5	5.7	17/10/02~04/12/02	300 KHz
STA 23	41°57.38'N	86°35.70'W	13.5	3.7	17/10/02~04/12/02	1200 KHz

^aDates are given as dd/mm/yy. ADCP at STA 21 did not work properly. Percent of cohesive sediment (silt+clay) was calculated by a polynomial fitting curve of the fraction data versus depth.

over water depth. The OBS sensor moored at STA 22 did not operate properly, while the OBS sensor at STA 23 only worked properly for the first half of the deployment period, so both ADCPs were calibrated with this data. Previous calibration data from similar locations generally fall within current calibration data. Figure 2 displays the calibration plot. Despite some scattered data, a distinct correlation between two sensors was found: R^2 value of the fitting curve was 0.75. This scatter is primarily attributed to the small sampling volume of the OBS. As might be expected, the calibration plot for the 300-KHz ADCP shows more scatter than the 1200-KHz data since it was not at the same location as the OBS. However, the calibration plot has a very similar trend with 1200 KHz except for having a much lower reference level (due to the different frequency). The baseline (minimum level) of ADCP signal strength repre-

sented background concentration was very consistent (within 3% error) and dependent on ADCP frequency. Since ADCP backscattering signal strength is known to respond nonlinearly to the amount of suspended materials while the OBS responds linearly, a second-order polynomial calibration curve was computed from the data in Figure 2,

$$C = a_1(S_v - S_0)^2 + b_1(S_v - S_0) + c_1, \quad (15)$$

where C is the suspended sediment concentration (mg/L), S_v is the back-scattering signal strength in dB, S_0 is the offset value depending on ADCP frequency, a_1 , b_1 , and c_1 are the calibration constants which are 0.0196, 3.5275, 160.25 for the 1200-KHz ADCP ($S_0 = 0$). The above equation was also applied to the 300-KHz ADCP with a different offset values, $S_0 = 25.83$, assuming the same calibration constants.

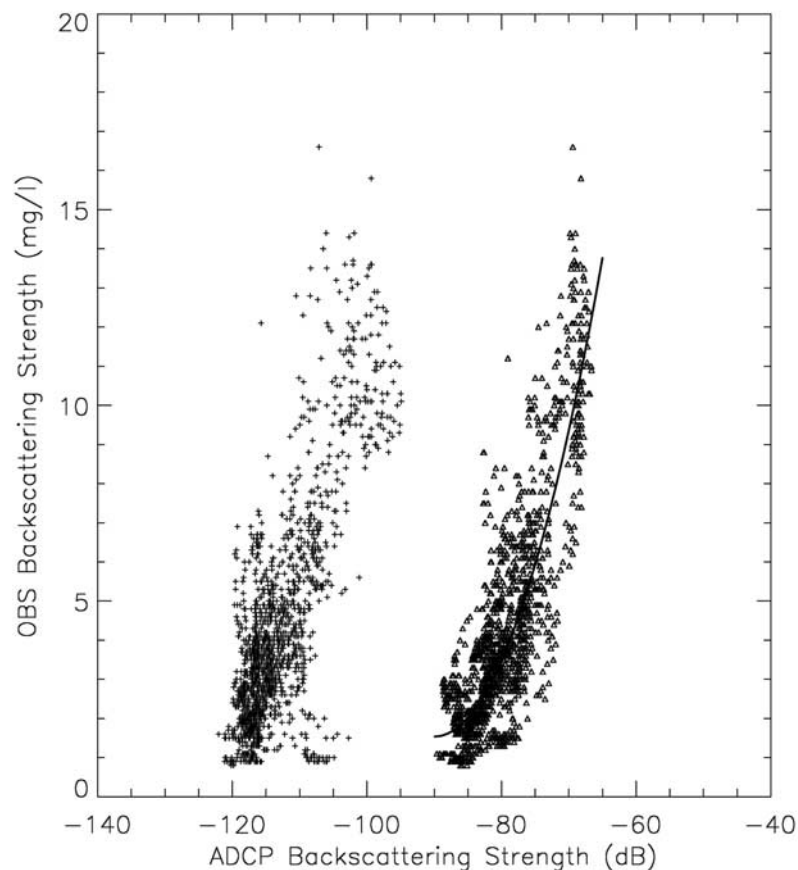


Figure 2. Calibration plot of ADCP backscattering strength with OBS backscattering strength. Plus signs, 300-KHz ADCP; open triangles, 1200-KHz ADCP.

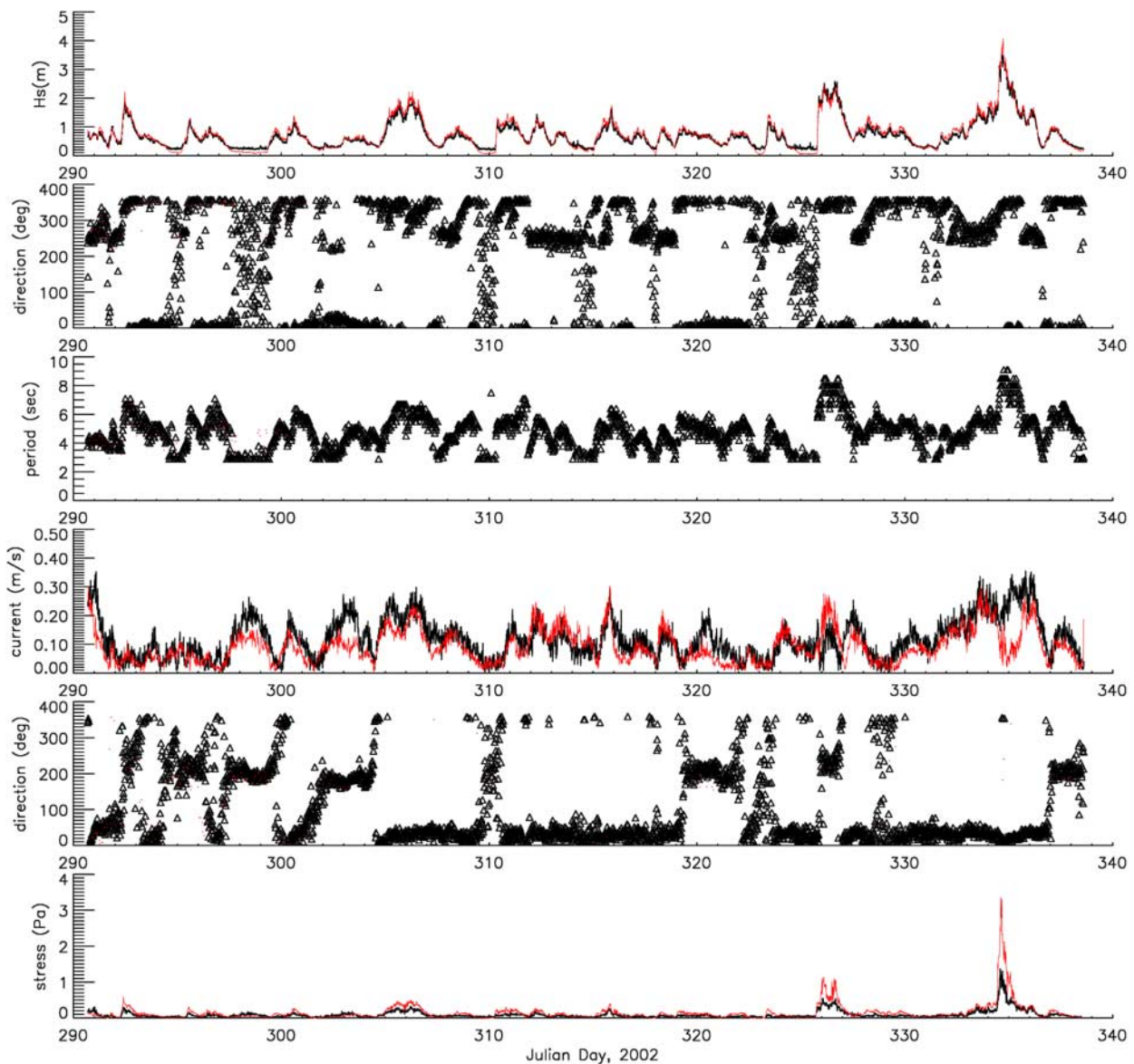


Figure 3. Measured wave height, direction, current speed, direction, and combined bed shear stress at STA 22 (black) and STA 23 (red) during October–December 2002.

Caution must be given when the concentrations are greater than 20 mg/L because the calibration data were all less than 20 mg/L.

[16] Figure 3 shows the measured waves, currents, and calculated bed stress at STA 22 and 23. The two sets of measurements are very similar, which indicates a very uniform wave field. Currents also have a similar pattern in direction and speed, but the magnitude at the offshore location (STA 22) was significantly larger (up to 30%) during some periods.

[17] Figure 4 displays the observed suspended sediment concentration profiles at STA 22 and 23. The observations are predominantly made up of fine-grained sediments since suspended sands are usually confined to the near-bed layer [Vincent and Green, 1990; Hay and Sheng, 1992]. The measurements were made far above that layer (1.6–3 m

above bed). The profiles show three distinct resuspension events (E1, E2, E3) at both stations and one event observed only at STA 23. These resuspension events are well correlated to the significant wave height. Since wave fields at the two locations were very similar, bed shear stresses were primarily dependent on water depths. Therefore the events in shallow water (STA 23) generally occurred earlier and lasted longer than those in deeper water (STA 22). Despite the large difference in bed shear stresses, the equivalent peak concentrations at the two locations are about the same (see Figure 6 in section 3.2), which shows the importance of sediment availability in resuspension.

3.2. Model Verification

[18] The sediment dynamics model described in section 2 with two size classes (1 floc + 1 sand) was calibrated with

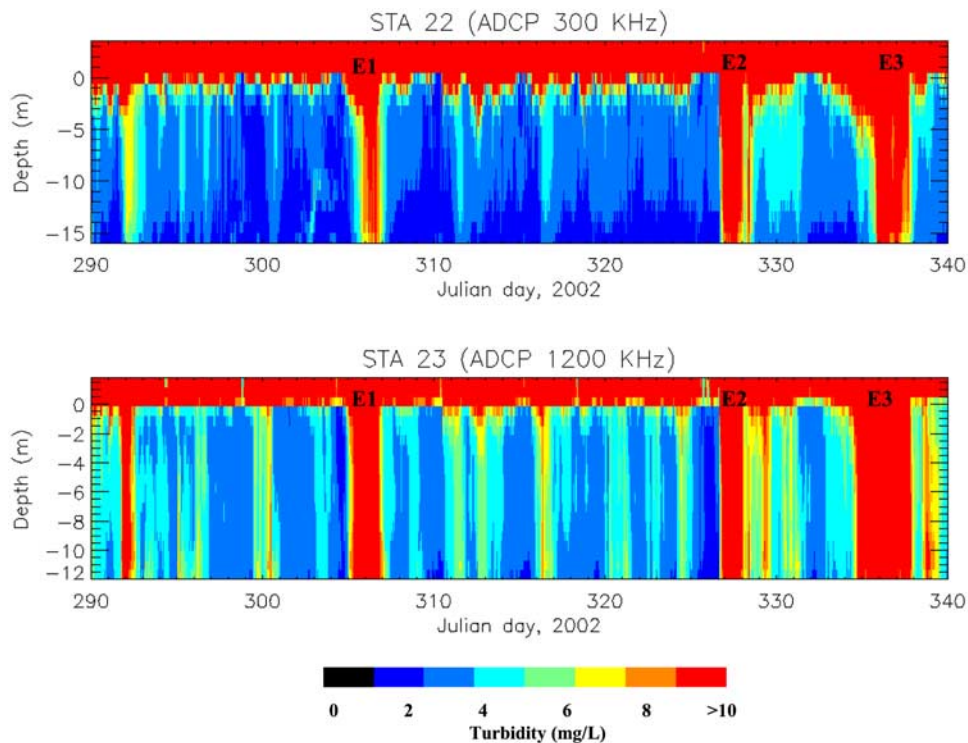


Figure 4. Suspended sediment profiles measured by ADCP during October–December, 2002.

the measurements at STA 23 and verified with the measurements at three other stations (STA 19, 20, and 22) without further adjustment of model input parameters (see Table 2). The initial background concentration was set to 2 mg/L close to a typical value in Lake Michigan. The calibration parameter values were in a physically reasonable range because they were based on numerous field observations in Lake Michigan. Results using three sand-size classes (100 μm , 200 μm , and 500 μm) were not significantly different from the results using a single size (250 μm). Since τ_c values for surface fine-grained sediment in the coastal region (5–50 m) are in the range of 0.05–0.15 Pa, the average value (0.10 Pa) was selected. A τ_{cd} value was chosen based on previous estimates [Krone, 1962; Mehta and Partheniades, 1975]. However, τ_{cd} is still poorly understood, and the data are sparse. It is also used for finer tuning of the model along with M_0 , changed in a physically reasonable way. The determination of the total available amount of fine-grained sediment (M_{coh}) in the active surface layer is an important consideration. The quantity might vary over time, space, and episodic events, depending on the local fraction of fine-grained sediment and the maximum

thickness of the active surface layer (Δz_{max}). Spatial distributions of the fine-grained fraction are easily measured (or estimated from a best-fit curve of the field data set), but it is extremely difficult to measure the thickness of the active surface layer. Therefore we determined Δz_{max} indirectly from the maximum concentration of fine-grained materials over the period including the several large resuspension events, assuming that all fine-grained materials in the active surface layer were resuspended ($\Delta z_{\text{max}} = C_{\text{max}} \times h / (f_{\text{cs}} \rho_b)$). The settling velocity of flocculated, fine-grained sediment is difficult to validate with field measurement. Previous laboratory and field measurement [Agrawal and Traykovski, 2001; Chakraborti and Atkinson, 2003] suggest an inverse relation between settling velocity and turbulent energy dissipation (or fluid shear). When fluid shear increases, flocs will be broken into small flocs usually resulting in slower settling speed. Some density increase will reduce the effect of size decrease on the settling speed. Our model result for a resuspension event (E3) shows the same trend (Figure 5). The settling speed of a median floc size (45–500 μm) is in the range of 4.5×10^{-4} m/s (39 m/day) $\sim 1.7 \times 10^{-4}$ m/s (14.7 m/day) over

Table 2. Input Parameters for Model Verifications (Two Size Class)

Input Parameters	Values
Sand size class (d_s)	250 μm
Floc size class (d_f)	Median floc size (calculated from equation (6))
Critical shear stress for erosion (τ_c)	0.1 Pa (fine-grained sediment), 0.21 Pa (sand)
Critical shear stress for fine-grained sediment deposition (τ_{cd})	1.5 Pa (fine-grained sediment)
Erosion rate constant (M_0)	0.001161 $\text{kg/m}^2 \text{ s Pa}$ (fine-grained sediment)
Initial fine-grained sediment fraction (f_{cs})	0.038 for STA 22, 0.057 for STA 23
Active surface layer thickness (Δz_{max})	5 mm

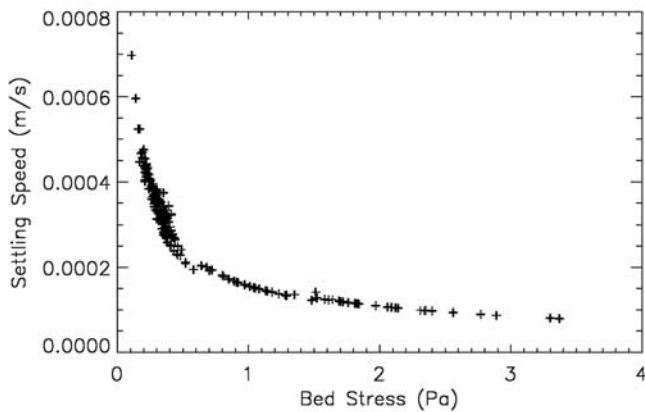


Figure 5. Model estimation of median settling velocity at the bed during an episodic event (E3) at STA 23.

the bed stress range (0.2~3.5 Pa). For other large events, the settling speed is in the similar range as it depends on the bed shear stress and concentration. The magnitude range is in good agreement with the estimation from the time variation of measured concentration. The particles smaller than the median size could stay in the water column for several days. To further verify our value of w_s , the settling flux from the model simulation was

compared to the measured settling flux from sediment trap data [Eadie *et al.*, 2002]. The measured mass flux data within the resuspension plume during 1996~1998 ranged from 30 g/m²/day to 880 g/m²/day for a corresponding C range of 10~40 mg/L measured during the same period. Since sediment traps were located at a certain height above the bed, the mass flux at the bed is expected to be higher than the measured range. The flux calculated by the model with $w_s = 4.5 \times 10^{-4}$ m/s was about 720 g/m²/d for C = 15 mg/L, which is the same order of magnitude as the measured flux. Therefore the evidence including the indirect estimation from C time series, satellite images, and comparison with measured mass flux indicates that the settling speed of the median floc size appears to be close to the true value.

[19] The time series of measured (C_m) and predicted (C_p) concentration at STA 19, STA 20, STA 22, and STA 23 are shown in Figure 6. The measured wave and current data were used as model inputs. Excellent agreement was achieved between the prediction and measurement for both stations STA 22 and STA 23. The root mean square values (RMS) of $C_p - C_m$, $\sqrt{(1/N) \sum (C_p - C_m)^2}$, were 0.93 and 1.13 for STA 22 and STA 23, respectively. Although more sophisticated statistics could be used to compare measured and predicted concentrations, we believe the RMS error is a sufficient indication of model accuracy for the purpose

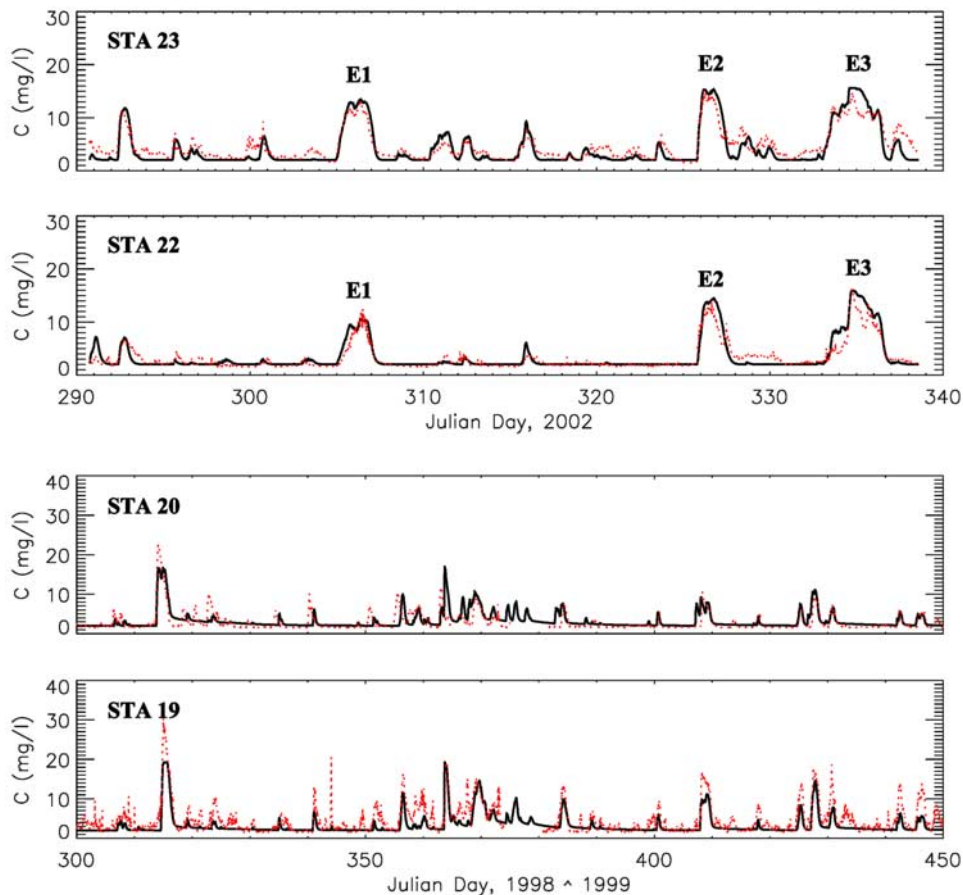


Figure 6. Comparison of model predictions (black solid line) with ADCP measurements (red dotted line) at four different stations during different time periods.

Table 3. Model Simulation Cases^a

Case	Sediment Availability	F_R ($\tau > \tau_c$)	F_S ($\tau < \tau_{cd}$)	Settling Velocity (w_s)	Sensitivity Parameter
C1	unlimited	$M(\tau - \tau_c)$	$w_s C(1 - \tau/\tau_{cd})$	5×10^{-4} m/s	$M/M_r = 0.012 \sim 1.0$ $M_r = f_{csr} M_0 = 4.37 \times 10^{-5}$ kg/m ² s Pa
C2	limited	$M(\tau - \tau_c)$	$w_s C(1 - \tau/\tau_{cd})$	5×10^{-4} m/s	$M/M_r = 0.012 \sim 2.75$ $M_r = f_{csr} M_0 = 4.37 \times 10^{-5}$ kg/m ² s Pa
C3	limited	$M(\tau - \tau_c)$	$w_s C(1 - \tau/\tau_{cd})$	flocculated	$M/M_r = 0.012 \sim 2.75$ $M_r = f_{csr} M_0 = 4.37 \times 10^{-5}$ kg/m ² s Pa
C4	limited	$f_{cs} M_0 (\tau - \tau_c)$	$w_s C(1 - \tau/\tau_{cd})$	$w_s = \text{constant}$	$w_s/w_{sr} = 0.1 \sim 20$ $w_{sr} = 5 \times 10^{-4}$ m/s
C5	limited	$f_{cs} M_0 (\tau - \tau_c)$	$w_s C(1 - \tau/\tau_{cd})$	flocculated	$\tau_{cd}/\tau_{cdr} = 0.033 \sim 2.0$ $\tau_{cdr} = 1.5$ Pa
C6	limited	$f_{cs} M_0 (\tau - \tau_c)$	$w_s C(1 - \tau/\tau_{cd})$	flocculated	$\tau_c/\tau_{cr} = 0.5 \sim 5.0$ $\tau_{cr} = 0.1$ Pa
C7	limited	$f_{cs} M_0 (\tau - \tau_c)$	$w_s C(1 - \tau/\tau_{cd})$	flocculated	$f_{cs}/f_{csr} = 0.2 \sim 2.0$ $f_{csr} = 0.038, 0.057$ for STA 22 and 23
C8	limited	$f_{cs} M_0 (\tau - \tau_c)$	$w_s C(1 - \tau/\tau_{cd})$	flocculated	size class and $M/M_0 = 0.125 \sim 3.0$

^aLimited: fine-grained sediments are confined to 5 mm top bed thickness. $M_0 = 0.001161$ kg/m²·s·Pa, $f_{cs} = 0.038, 0.057$ for STA 22 and 23 (initial value). C1~C6: two size class (median floc size + 250 μ m sand) was used. C7: two size class (median floc size + 250 μ m sand) and six size class (three floc size class + 100, 200, 500 μ m sand) were used.

of this paper. The model predicted three large resuspension events ($C_m > 10$ mg/L) with good agreement in magnitude, phase, and detailed features. Small-scale resuspension events were generally predicted well but overpredicted in some cases. The prediction of a small-scale event is generally more difficult than a large event because the resuspension due to second-order processes (such as current, the interaction between wave and current, uncertainty in critical shear stress, particle size distribution, and so on) tends to be equivalent to or more important than the effect of wave-induced bed stress. A notable observation is the similar magnitudes of maximum suspended concentration (C_{\max}) during three distinct events (E1, E2, E3) regardless of significant differences in bed shear stresses ($\tau_{b,STA22}/\tau_{b,STA23} = 0.66, 0.48, 0.40$ for E1, E2, E3); C_{\max} was in the range from 14 to 17 mg/L. Furthermore, during a more severe storm event (E3), C_{\max} at STA 22 was about 4 mg/L higher than at STA 23; note that the bed shear stress ratio during E3 was 0.4. These observations suggest that C_{\max} might be primarily limited by the available amount of fine-grained materials. More detailed discussion will be made in the next section.

[20] To verify the model and the methodology of ADCP measurement in section 3.1, other ADCP data at STA 19 (300 KHz) and STA 20 (1200 KHz) were compared with model results with the same resuspension parameter values. Since these ADCPs were not the same ADCPs at STA 22 and STA 23 and were incapable of measuring wave parameters, the pressure data recorded at nearby St. Joseph (about 10 km away from measurement locations) were used to extrapolate wave parameters. These pressure data were less reliable in estimating wave parameters than ADCP measurement. The same system constants and calibration equation were used to obtain C_m . Overall, ADCP measurements and the model results were in fairly good agreement, showing good predictions of resuspension events in phase and magnitude unless $C_m > 15$ mg/L. The RMS values of $C_p - C_m$, for STA 19 and STA 20 equal to 1.80 and 1.53, respectively. The model tended to underpredict C for large storm events ($C_m > 15$ mg/L). The underprediction may be either from overestimation of C_m by the ADCP calibration curve or from underestimation of wave parameters. Both causes were possible because the ADCP calibration equations were obtained with a limited data set (0~20 mg/L) and wave data were not measured at the same location or with the same reliability as the ADCP measurement. Another possible reason might be due to the uncertainty of the resuspension parameters such as f_{cs} which could be different for different sites. However, the comparison

appears to be adequate to validate our model with the measurements for the purpose of the current study.

3.3. Effects of Resuspension Parameters

[21] Model sensitivity analysis was performed to explore the effects of resuspension parameters (P_r) on the predictions by running the model for eight simulation cases (see Table 3). Several different model formulations were tested over a range of nondimensionalized resuspension parameters (M/M_r , w_s/w_{sr} , τ_{cd}/τ_{cdr} , τ_c/τ_{cr} , f_{cs}/f_{csr} , size distribution). Model formulations can be mainly divided into four different categories: (1) unlimited versus limited sediment source; (2) constant settling versus flocculated settling; (3) constant erosion rate versus fraction dependent erosion rate; and (4) two size class versus six size class. The reference resuspension parameter values (denoted by subscript “r”) are the values in Table 2. M_r (used in C1, C2, and C3) was determined from $f_{cs} M_0$ to make the entrainment rate comparable to the other cases. All reference values are in a physically reasonable range. The resulting predictions of C time series at STA 22 and STA 23 are compared to measurements (red dotted line) in Figures 7 and 8. The corresponding RMS errors are plotted against the variation of the normalized resuspension parameter being tested (Figure 9).

[22] Cases C1–C3 examine unlimited (C1) versus limited (C2) sediment availability, constant settling (C2) versus flocculated settling (C3), and sensitivity to the erosion rate constant (M). Case C1 (unlimited sediment availability) shows the extraordinary underprediction and overprediction of C during the three large resuspension events with the erosion rate constant values, $M/M_r = 0.012$ and 1.0, respectively (blue and black solid line). The best results can be obtained at $M/M_r = 0.06$ and 0.3 for STA 23 and STA 22, respectively, but they significantly underpredict C time series (green solid line). The results for unlimited sediment source are expected as the resuspension flux (F_R) increases linearly with bed shear stress. Instead of adjusting M , the RMS error can be improved by increasing the settling velocity, w_s . However, the result was similar to the underprediction case (green solid line), and the w_s value was much larger than the value estimated from the measurement. Other adjustments of resuspension parameters did not improve the prediction. On the basis of results in C1, we conclude that the source of fine-grained sediment is limited. In case C2 (limited sediment availability) the F_R and F_D terms and other input parameter values are exactly the same as those in C1. The result is much improved when compared to C1, and the adjustment

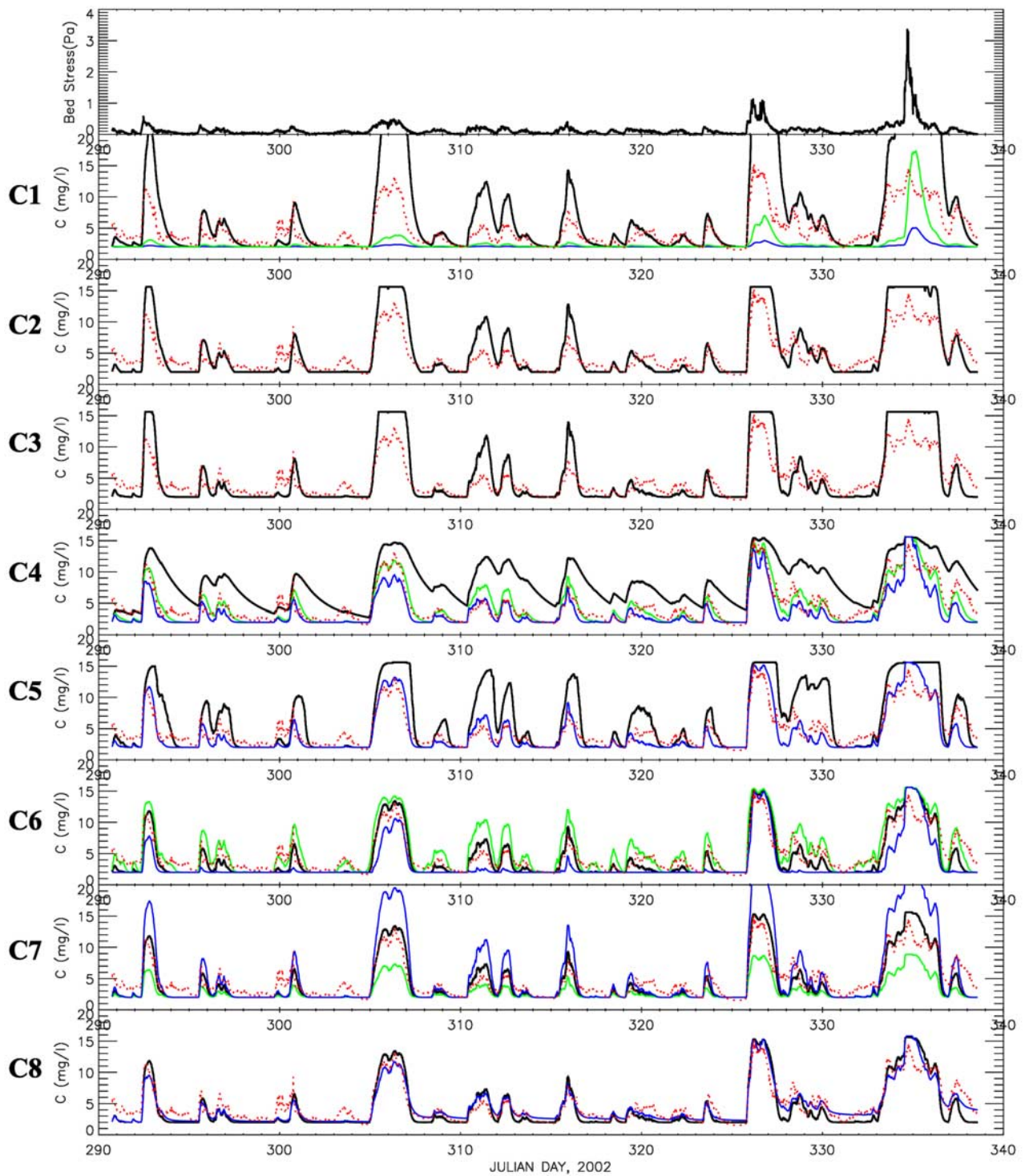


Figure 7. Time series of bed stress and suspended concentration for different model formulations (C1~C8) at STA 23. Red dotted line indicates the measurements. C1: unlimited source, blue ($M/M_r = 0.012$), green ($M/M_r = 0.06$), black ($M/M_r = 1.0$); C2: limited source, constant settling velocity, black ($M/M_r = 1.0$); C3: limited source, flocculated settling velocity, black ($M/M_r = 1.0$); C4: limited source, dependent on f_{cs} , black ($w_s/w_{sr} = 0.2$), green ($w_s/w_{sr} = 1.0$), blue ($w_s/w_{sr} = 2.0$); C5: limited source, black ($\tau_{cd}/\tau_{cdr} = 0.067$), blue ($\tau_{cd}/\tau_{cdr} = 1$); C6: limited source, green ($\tau_c/\tau_{cr} = 0.5$), black ($\tau_c/\tau_{cr} = 1.0$), blue ($\tau_c/\tau_{cr} = 2.0$); C7: limited source, green ($f_{cs}/f_{csr} = 0.5$), black ($f_{cs}/f_{csr} = 1.0$), blue ($f_{cs}/f_{csr} = 1.5$); C8: limited source, black (median floc size + sand), blue (3 floc size class + sand).

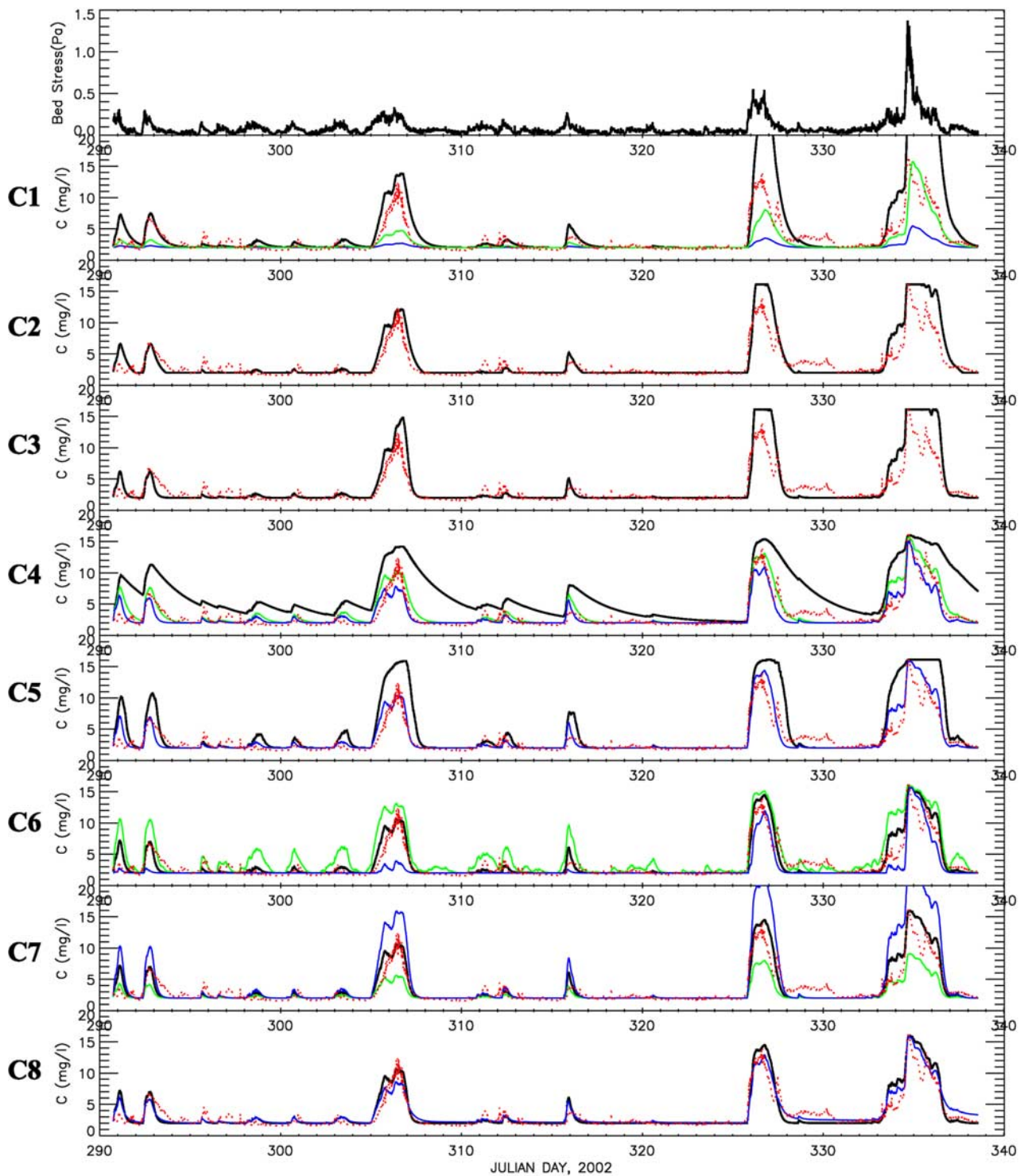


Figure 8. Time series of bed stress and suspended concentration for different model formulations (C1~C8) at STA 22. Red dotted line indicates the measurements. C1: unlimited source, blue ($M/M_r = 0.012$), green ($M/M_r = 0.3$), black ($M/M_r = 1.0$); C2: limited source, constant settling velocity, black ($M/M_r = 1.0$); C3: limited source, flocculated settling velocity, black ($M/M_r = 1.0$); C4: limited source, dependent on f_{cs} , black ($w_s/w_{sr} = 0.2$), green ($w_s/w_{sr} = 1.0$), blue ($w_s/w_{sr} = 2.0$); C5: limited source, black ($\tau_{cd}/\tau_{cdr} = 0.067$), blue ($\tau_{cd}/\tau_{cdr} = 1$); C6: limited source, green ($\tau_c/\tau_{cr} = 0.5$), black ($\tau_c/\tau_{cr} = 1.0$), blue ($\tau_c/\tau_{cr} = 2.0$); C7: limited source, green ($f_{cs}/f_{csr} = 0.5$), black ($f_{cs}/f_{csr} = 1.0$), blue ($f_{cs}/f_{csr} = 1.5$); C8: limited source, black (median floc size + sand), blue (3 floc size class + sand).

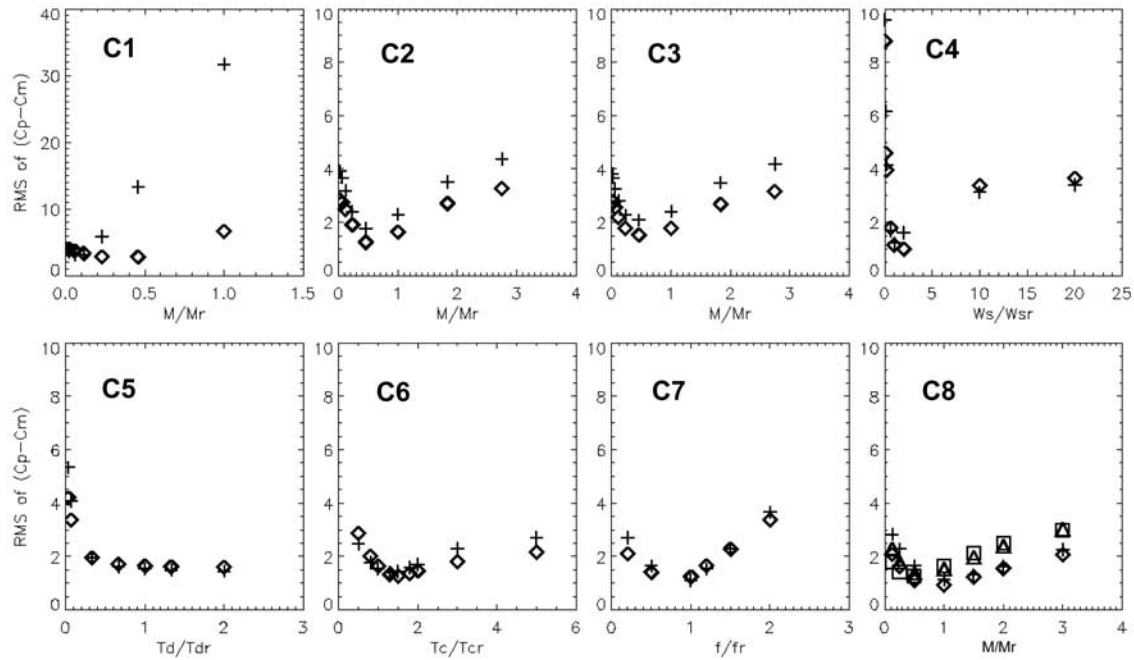


Figure 9. Model sensitivity analysis of resuspension parameters for unlimited (C1) and limited source (C2~C8). C1~C7: STA 22 (plus signs), 23 (open diamonds), C8: STA 22 (two size class: open squares; four size class: open triangles), 23 (two size class: plus signs; four size class: open diamonds).

of M to $M/M_r = 0.46$ gave a better result (lower RMS value) as shown in Figure 9. However, the predictions show a constant C after depleting all available sediment until the flow condition is in favor of net settling, which is not seen in the measurements.

[23] The simulation cases C2–C3 display the model prediction with constant settling (C2) versus flocculated settling (C3) with limited sediment source. All other resuspension parameter values are set to be the same. Both predictions give very similar results because the averaged flocculated settling velocity is very close to the constant settling velocity in C2. However, C3 results tend to be lower in concentration right after an event due to flocculated settling in the lower turbulent environment. The flocculation process may not be crucial in the first-order prediction if the averaged settling velocity is estimated properly.

[24] Next we tested the dependence of entrainment rate on remaining fine-grained sediment fraction (f_{cs}) and the effect of settling velocity. The initial f_{cs} was determined from field observation for each site and was not changed. This case, C4, was run for the different constant settling velocities ($w_s/w_{sr} = 0.02, 0.1, 0.2, 0.6, 1.0, 2.0, 10, 20$). The other resuspension parameter values are same as C2. The black, green, and blue solid lines in the plot indicate the run with $w_s/w_{sr} = 0.2, 1.0, \text{ and } 2.0$, respectively. The green line ($w_s/w_{sr} = 1.0$) is in excellent agreement with measurements (red dotted line) for both stations. The RMS errors were 1.15 and 1.23 for STA 22 and STA 23, respectively. As the only difference between C2 and C4 is the dependence of entrainment rate on f_{cs} , we can say that the inclusion of f_{cs} in F_R is critical for a successful prediction. Unless a bed surface is completely covered by fine-grained materials, the probability of entrainment for fine-grained materials must be dependent on its fraction, f_{cs} . Some uncertainty

exists due to integrating f_{cs} over the top surface layer in the current field data. The top submillimeter layer presumably has higher f_{cs} than the first centimeter of sediment bed but in situ measurement is not practically possible.

[25] The case C4 in Figure 9 shows the effect of settling speed on the model prediction. Interestingly, the RMS error curve has an uneven parabola shape with a lower slope for increasing w_s/w_r after a critical point, $w_s/w_r \sim 1.2$. A 50% reduction ($w_s/w_r = 0.5$) of w_s increases the RMS error about 68% while the increase of w_s above the best-fit value has less effect on the model prediction. The reason could be explained by an exponential decrease of C with increasing w_s in a simple solution of the differential equation (1) assuming constant parameters, leading to

$$C \sim F_R/w_s + c_1 \exp(-w_s t). \quad (16)$$

Therefore, after a critical point, the effect of w_s is reduced more and more with its increase. The RMS error curve reflects that the absolute magnitude of settling speed is also very important along with f_{cs} . The magnitude of w_s appears to determine first-order features and accuracy of the prediction if the other parameter values are appropriately selected.

[26] The simulation cases C5, C6, C7, and C8 were designed to investigate the effects of other resuspension parameters (flocculated settling velocity, critical shear stress for deposition, critical shear stress for entrainment, variation of initial fine-grained sediment fraction, and floc size distribution) on the results of model with f_{cs} dependent erosion rate and limited sediment availability. In the simulation case C5, if the blue line ($w_s = \text{variable}, \tau_{cd} = 1.5 \text{ Pa}$) is compared to the green line ($w_s = \text{constant}$) in C4, there is no significant difference between them; note that other

resuspension parameter values are the same. The slightly higher concentration during three large events is attributed to the lower settling speed in C5; as plotted in Figure 5, the settling speed of the median floc size ranged from 1×10^{-4} m/s to 5×10^{-4} m/s according to the bed shear stress. The result (with flocculated settling) shows a slight reduction in RMS error without any other significant difference, as demonstrated in the previous comparison of C2–C3. The black and blue solid lines in C5 denotes the model prediction with $\tau_{cd} = 0.1$ and 1.5 Pa ($\tau_{cd}/\tau_{cdr} = 0.067$ and 1) and Figure 9 (C5) displays the RMS error curve with τ_{cd}/τ_{cdr} . Typical range of reported τ_{cd} is $0.05 \sim 1.5$ Pa. The RMS curves suggest that the decreasing τ_{cd} in range of $0.05 \sim 1.0$ Pa rapidly increase the error in model prediction and the increasing τ_{cd} in range of $1.0 \sim 3.0$ Pa does not significantly affect the prediction.

[27] The simulation case, C6, shows the effect of critical shear stress, τ_c . The green, black, and blue solid lines indicate the model predictions for $\tau_c = 0.05, 0.1,$ and 0.2 Pa ($\tau_c/\tau_{cr} = 0.5, 1.0, 2.0$). The prediction with $\tau_c = 0.05$ Pa was generally higher than the measured concentration. Especially, it significantly overpredicted the concentration for the relatively weak resuspension events. The prediction with $\tau_c = 0.2$ Pa was generally lower than the measured concentration and did not predict the weak resuspension events obviously observed in the measurement. The overprediction and missing of weak resuspension events reflects that τ_c must be in the range of $0.05 \sim 0.2$ Pa. This estimation of τ_c agrees well with other observations from the tripod measurements. The RMS error curve has a slightly uneven parabola shape setting. Here $\tau_c = 0.05$ Pa may cause about 80% increase of RMS error.

[28] The simulation cases, C7 and C8, show the effect of initial fine-grained sediment fraction (f_{cs}) on model prediction. In these runs, the initial condition of f_{cs}/f_{csr} was changed from 0.20 to 2.0 . The green, black, and blue solid lines denote the model predictions with $f_{cs}/f_{csr} = 0.5, 1.0,$ and 1.5 , respectively. The higher f_{cs} overpredicts the measurement, while the lower f_{cs} underpredicts. As $dC/dt \propto f_{cs}$ in equation (1), the RMS error tends to increase linearly with decreasing or increasing f_{cs}/f_{csr} from the best fit point. Relative average uncertainty of f_{cs} in southern Lake Michigan data set could be estimated as

$$\sqrt{\sum (f_{cs,i} - \hat{f}_{cs})^2 / N} / \hat{f}_{cs}, \quad (17)$$

where $f_{cs,i}$ is the measured size fraction for each sampling location, \hat{f}_{cs} is the estimated size fraction from a regression curve for each sampling location, and N is the number of data points. The value was approximately $\pm 13\%$ at $\hat{f}_{cs} = 50\%$, tending to increase up to roughly $\pm 50\%$ (equivalent to $f_{cs}/f_{csr} = 0.5$ or 1.5) at $\hat{f}_{cs} = 10\%$. The plots of RMS error versus f_{cs}/f_{csr} in Figure 9 (C7) have the largest slope ($=\Delta(\text{RMS error})/\Delta(f_{cs}/f_{csr})$) among the resuspension parameters, indicating that f_{cs} is a very sensitive parameter significantly affecting model results. Fifty percent change of f_{cs} causes about 130% increase in RMS error, which was the largest change among the parameters. Practically, sediment resuspension occurs over a large area; therefore the f_{cs} value should be spatially averaged over some scale. This averaging reduces the uncertainty effect due to the

local variability of f_{cs} . In addition to the averaging effect, a possible maximum RMS error might be significantly reduced, provided more accurate measurement of f_{cs} .

[29] The simulation case, C8, explains the effect of floc size distribution. The black solid line utilized a median floc size to calculate w_s while the blue solid line corresponds to a simulation with three floc size classes to calculate the spectrum of w_s . Overall, size distribution appears to be insignificant in predicting the resuspension events. However, it appears to be very important for the prediction of the lingering particles staying for $2 \sim 3$ days after a large resuspension event. The measured particle size distribution at 1 m above bottom reflects that the flocs sizes have a wide range and small size flocs may remain in suspension for several days after a large event [Winkelman *et al.*, 1998]. If we compare time series data for the two runs, the three size class simulation predicts well the concentration right after the large resuspension events (E2, E3), while the one size class simulation underpredicts it. Therefore floc size distribution changing with turbulent characteristics seems to have a more important effect on second-order features in C time series, enhancing the further transport of very fine materials after an event.

4. Summary and Conclusions

[30] To identify and compare quantitatively the important parameters for sediment resuspension in the coastal area of southern Lake Michigan, a sensitivity analysis was performed using a one-dimensional sediment resuspension model capable of dealing with the mixed sediment type common in the area. The model was compared to ADCP measurement of suspended materials during the fall of 2002.

[31] The sensitivity analysis showed that the most sensitive parameter is the fraction of fine-grained materials (f_{cs}) and sediment availability. The entrainment rate is limited by the available amount of fine-grained materials in the active top surface layer. This finding appears to explain the relatively uniform distribution of sediment concentration across the resuspension plume in which the bed shear stress distribution is nonuniform (much higher in shallow region than deep region). In many modeling studies, the f_{cs} is set to a constant over the study area and the critical shear stress (τ_c) is used as a calibration parameter to control the resuspension rate, which often results in unrealistic τ_c value and incorrect predictions. Fortunately, f_{cs} is much easier to measure than τ_c . Therefore it is important to use the measured f_{cs} as model input data.

[32] Other resuspension parameters are also found to be important. Among them, the absolute magnitude of settling speed is crucial in controlling the first-order prediction. The spectrum of settling velocity has a less significant effect, except for the prediction of the lingering small particles right after a large event. Within the measurement uncertainty of a parameter, the model prediction can cause up to about 40% difference of suspended concentration averaged over the time period in the present case. Interestingly, all parameters have similar sensitivity (slope of RMS error curve) when they are reduced below the best-fit point, while they display significant differences when they are increased about the optimal value. In particular, the model

is not very sensitive to an increasing settling velocity from the best-fit point.

[33] It still remains in question to determine accurately the total amount of fine-grained sediment in the active surface bed layer available to a resuspension event. The availability may vary over time and space. We still do not know enough about what amount of and when fine-grained materials come from sources (bluff erosion) and how they redistribute from nearshore to deeper parts of the coastal region. These issues are remained for better prediction of long-term sediment transport in southern Lake Michigan.

Notation

C	depth-averaged sediment concentration;
C_A	advective component of C ;
C_L	local component of C ;
C_D	drag coefficient;
C_{FD}	effective settling coefficient for particle shape;
C_i	concentration for each size class;
C_{eq}	depth-averaged equilibrium concentration;
C_m	measured concentration;
C_{max}	maximum concentration;
C_p	predicted concentration;
ΔC_{RMS}	Relative RMS error of $C_p - C_m$;
d_f	floc size distribution;
d_{fm}	median floc diameter;
d_s	sediment diameter;
d^*	non-dimensional sediment diameter;
F_A	advective flux;
F_D	deposition flux;
F_L	lateral flux;
F_R	resuspension flux;
$f_{f,I}$	fraction of each floc size class (modeled);
f_{cs}	fraction of fine-grained sediment in bed;
$f_{cs,I}$	fraction of fine-grained sediment in size class I;
f_{cs}	fraction of fine-grained sediment estimated from a regression curve;
$f_{ns,I}$	fraction of sand for each size class;
f_w	wave friction factor;
$F(R, \sigma_d)$	function that converts C to the concentration at the deposition level;
g	acceleration due to gravity;
G	fluid shear velocity at the reference level;
h	water depth;
M	resuspension rate coefficient without f_{cs} ;
M_0	resuspension rate coefficient with f_{cs} ;
M_r	reference resuspension rate coefficient;
N	number of data points;
n_c	number of floc size class;
n_s	number of sand size class;
$P_{D,I}$	probability distribution function for deposition of each size class I;
P_r	resuspension parameters;
R	Rouse number;
S_0	offset for ADCP backscatter calibration;
S_v	back-scattering signal strength;
t	time;
U	depth-averaged velocity;
u^*_{cw}	shear velocity;
w_{si}	settling velocity of each floc size class;

z	height above the bed;
z_b	bed layer thickness;
Δz	thickness of active surface layer;
Δz_{max}	maximum thickness of active surface layer;
α_0	experimental constant;
ρ_b	bed bulk density;
ρ_f	floc density;
ρ_s	sediment density;
ρ_w	water density;
σ_d	deposition level;
σ_r	reference level;
τ_b	bed shear stress;
τ_c	critical shear stress for erosion;
τ_{cr}	reference critical shear stress for erosion;
τ_{cd}	critical shear stress for deposition;
τ_{cdr}	reference critical shear stress for deposition;
τ_{cw}	bed stress due to waves and currents;
τ_{wm}	maximum wave stress;
ν_m	mixture viscosity.

Appendix A

[34] Consider the approximation to the sediment advection-diffusion equation for horizontally uniform distribution. The governing equation is reduced to

$$\frac{\partial(HC)}{\partial t} = \frac{\partial}{\partial z} \left(\frac{K_v}{H} \frac{\partial C}{\partial z} + w_s C \right). \quad (A1)$$

Integrating (A1) over the water depth,

$$\frac{\partial(H\bar{C})}{\partial t} = J_0 - J_1, \quad (A2)$$

where J_0 is the net sediment flux at bottom boundary and J_1 is the net sediment flux at water surface boundary which is assumed to be negligible.

Subtracting (A2) from (A1) gives

$$\frac{\partial(HC')}{\partial t} = \frac{\partial}{\partial z} \left(\frac{K_v}{H} \frac{\partial C}{\partial z} + w_s C \right) - J_0. \quad (A3)$$

Assuming that $\partial_t(HC') < \partial_t(H\bar{C})$, the equation (A3) is approximated by

$$\frac{\partial}{\partial z} \left(\frac{K_v}{H} \frac{\partial C}{\partial z} + w_s C \right) = J_0. \quad (A4)$$

Integrating (A4) once over z ,

$$\frac{K_v}{H} \frac{\partial C}{\partial z} + w_s C = J_0(z - 1). \quad (A5)$$

By assuming the turbulent diffusivity, $K_v/H = u^* \kappa z$, and equilibrium conditions ($C = C_{eq}$ and $J_0 = 0$) at $z = z_{eq}$, the solution of the first-order differential equation (A5) is given,

$$C = \left(\frac{z_{eq}}{z} \right)^R C_{eq} - \left(1 - \frac{Rz}{1+R} \right) \frac{J_0}{w_s}, \quad (A6)$$

where Rouse number, $R = w_s/u^* \kappa$.

[35] For sand under nonequilibrium conditions, the net flux is given as

$$J_0 = w_s \left(\frac{1+R}{1+R(1-z_{eq})} \right) (C_{eq} - C_{ne}), \quad (A7)$$

where C_{ne} is the actual concentration at the reference equilibrium level. To express (A7) in terms of the depth averaged sediment concentration (\bar{C}), the integration of (A7) over the water depth gives

$$J_0 = w_s \left(\frac{2(1+R)}{2+R(1-z_{eq})} \right) (\bar{C}_{eq} - \bar{C}_{ne}), \quad (A8)$$

where

$$\bar{C}_{eq} = \frac{\ln(z_{eq}^{-1})}{(z_{eq}^{-1} - 1)} C_{eq}, \quad R = 1 \quad (A9)$$

$$\bar{C}_{eq} = \frac{(z_{eq}^{R-1} - 1)}{(1-R)(z_{eq}^{-1} - 1)} C_{eq}, \quad R \neq 1.$$

The equilibrium concentration for average sand size class at reference level is expressed by *Smith and McLean's* [1977] formula as follows:

$$C_{eq} = \rho_s \frac{0.65\gamma_0 T}{1 + \gamma_0 T}, \quad T = \frac{\tau_b - \tau_c}{\tau_c}, \quad (A10)$$

where γ_0 is a constant equal to 2.4×10^{-3} .

[36] The equation (A8) is applied for the arbitrary number of sand size class (n_s) as follows:

$$J_0 = F_R - F_D = \sum_{i=1}^{n_s} w_{s,i} f(R, \sigma_r) [f_{ns,i} \bar{C}_{eq} - \bar{C}_i], \quad (A11)$$

where n_s is the number of sand size classes, $f(R, \sigma_r) = 2(1+R)/(2+R(1-z_{eq}))$ with $\sigma_r = z_{eq}$, \bar{C}_i is the depth average concentration for each sand size class, and $f_{ns,i}$ is the fraction of each sand size class.

[37] For fine-grained sediments, the deposition flux is given as

$$F_D = \begin{cases} w_s C_d \left(\frac{\tau_{cd} - \tau_b}{\tau_{cd}} \right) = w_s P_d C_d & \tau_b < \tau_{cd} \\ 0 & \tau_b > \tau_{cd}, \end{cases} \quad (A12)$$

where C_d is the fine-grained sediment concentration at deposition level (σ_d), and τ_{cd} is the critical stress for deposition which depends on floc properties. Inserting (A12) into the solution of differential equation (A5) and evaluating the integration constant at the deposition level, we can get

$$C = \left(1 - \frac{Rz}{1+R} \right) P_d C_d + \left(1 - \left(1 - \frac{Rz_d}{1+R} \right) P_d \right) C_d \frac{z_d^R}{z^R}. \quad (A13)$$

Integrating (A13) over the water depth, we can get

$$C_d = \left(\left(\frac{2+R(1-z_d)}{2(1+R)} \right) P_d + \frac{\ln(z_d^{-1})}{(z_d^{-1} - 1)} \cdot \left(1 - \left(\frac{1+R(1-z_d)}{1+R} \right) P_d \right) \right)^{-1} \bar{C}, \quad R = 1 \quad (A14)$$

$$C_d = \left(\left(\frac{2+R(1-z_d)}{2(1+R)} \right) P_d + \frac{(z_d^{R-1} - 1)}{(1-R)(z_d^{-1} - 1)} \cdot \left(1 - \left(1 - \frac{Rz_d}{1+R} \right) P_d \right) \right)^{-1} \bar{C}, \quad R \neq 1. \quad (A15)$$

[38] If the above derivations are applied to the resuspension and deposition flux formula for the arbitrary numbers of floc size class, the net flux gives

$$J_0 = F_R - F_D = \sum_{i=1}^{n_c} (f_{f,i} f_{cs} M_0 (\tau_b - \tau_c) - w_{s,i} f(R, \sigma_d) \bar{C}_i P_{d,i}), \quad (A16)$$

where $f(R, \sigma_d)$ is the converting function in (A14) and (A15) that converts the depth-averaged concentration to the concentration at the deposition level ($\sigma_d = z_d$), \bar{C}_i is the depth average concentration for each floc size class, $f_{f,i}$ is the fraction of each floc size class in water column, and f_{cs} is the fraction of fine-grained sediments in bed.

[39] **Acknowledgments.** The authors are indebted to B. J. Eadie for providing sediment data and his helpful comments. The authors also would like to thank G. Miller and M. McCormick for providing ADCP data during 1998~2000 and for their assistance in interpreting the data.

References

- Agrawal, Y. C., and P. Traykovski (2001), Particles in the bottom boundary layer: Concentration and size dynamics through events, *J. Geophys. Res.*, *106*(C5), 9533–9542.
- Beletsky, D., D. J. Schwab, M. J. McCormick, G. S. Miller, J. H. Saylor, and P. J. Roebber (2000), Hydrodynamic modeling for the 1998 Lake Michigan coastal turbidity event, paper presented at Sixth International Conference on Estuarine and Coastal Modeling, Am. Soc. of Civ. Eng., New Orleans, La.
- Brooks, A. S., and D. N. Edgington (1994), Biogeochemical control of phosphorus cycling and primary production in Lake Michigan, *Limnol. Oceanogr.*, *39*, 962–968.
- Chakraborti, R. K., and J. F. Atkinson (2003), Determination of particle settling rate and characterization of particulate structure using an image analysis method, paper presented at 46th Conference on Great Lakes Research, 10th World Lake Conference, Int. Assoc. for Great Lake Res., Chicago, Ill.
- Chambers, R. L., and B. J. Eadie (1980), Nearshore chemistry in the vicinity of the Grand River, Michigan, *NOAA Tech. Memo. ERL GLERL-28*, pp. 23–26, Natl. Oceanic and Atmos. Admin., Silver Spring, Md.
- Deines, K. L. (1999), Backscatter estimates using broadband acoustic Doppler current profilers, paper presented at Sixth Working Conference on Current Measurement, Inst. of Electr. And Electron. Eng., San Diego, Calif.
- Eadie, B. J., and S. L. Lozano (1999), Grain size distribution of the surface sediments collected during the Lake Michigan mass balance and environmental mapping and assessment programs, *NOAA Tech. Memo. ERL GLERL-III*, pp. 4–25, Natl. Oceanic and Atmos. Admin., Silver Spring, Md.
- Eadie, B. J., and J. A. Robbins (1987), The role of particulate matter in the movement of contaminants in the Great Lakes, in *Sources and Fates of Aquatic Pollutants*, ACS Adv. Chem. Ser., vol. 216, edited by R. Hites and S. Eisenreich, pp. 319–364, Am. Chem. Soc., Washington, D. C.
- Eadie, B. J., R. L. Chambers, W. S. Gardner, and G. L. Bell (1984), Sediment trap studies in Lake Michigan: Resuspension and chemical fluxes in the southern basin, *J. Great Lakes Res.*, *10*, 307–321.

- Eadie, B. J., et al. (2002), Particle transport, nutrient cycling, and algal community structure associated with a major winter-spring sediment resuspension event in southern Lake Michigan, *J. Great Lakes Res.*, 28, 324–337.
- Gailani, J., C. K. Ziegler, and W. Lick (1991), Transport of suspended solids in the Lower Fox River, *J. Great Lakes Res.*, 17, 479–494.
- Harris, C. K., and P. L. Wiberg (2002), Across-shelf sediment transport: Interaction between suspended sediment and bed sediment, *J. Geophys. Res.*, 107(C1), 3008, doi:10.1029/2000JC000634.
- Harris, C. K., C. R. Sherwood, J. C. Warner, and P. L. Wiberg (2003), Sediment bed limits to resuspension and transport with application for the northwestern Adriatic, paper presented at 7th International Conference on Nearshore and Estuarine Cohesive Sediment Transport Process, Va. Inst. of Mar. Sci., Gloucester, Va.
- Hawley, N., and C. H. Lee (1999), Sediment resuspension and transport in Lake Michigan during the unstratified period, *Sedimentology*, 46, 791–806.
- Hawley, N., and B. M. Lesht (1995), Does resuspension maintain the benthic nepheloid layer in southeastern Lake Michigan?, *J. Sediment. Res., Sect. A*, 65, 69–76.
- Hay, A. E., and J. Sheng (1992), Vertical profiles of suspended sand concentration and size from multifrequency acoustic backscatter, *J. Geophys. Res.*, 97(C10), 15,661–15,677.
- Jonsson, I. G. (1966), Wave boundary layers and friction factors, paper presented at 10th International Conference on Coastal Engineering, Am. Soc. of Civ. Eng., Tokyo.
- Justesen, P. (1988), Turbulent wave boundary layers, *Ser. Pap. 43*, Inst. of Hydrodyn. and Hydraul. Eng., Tech. Univ. of Denmark, Lyngby, Denmark.
- Kamphuis, J. W. (1975), Friction factors under oscillatory waves, *J. Waterw. Harbors Coastal Eng. Div. Am. Soc. Civ. Eng.*, 101, 135–144.
- Krone, R. B. (1962), Flume studies of the transport of sediment in estuarial shoaling processes, Ph.D. thesis, Hydraul. Eng. Lab. and Sanit. Eng. Lab., Univ. of Calif. at Berkeley, Berkeley.
- Lee, C. G., C. H. Wu, and J. A. Hoopes (2004), Automated sediment erosion testing system using digital imaging, *J. Hydraul. Eng.*, 130(8), 771–782.
- Lick, W., and J. Lick (1988), Aggregation and disaggregation of fine-grained lake sediments, *J. Great Lakes Res.*, 14, 514–523.
- Lick, W., and J. McNeil (2001), Effects of sediment bulk properties on erosion rates, *Sci. Total Environ.*, 266, 41–48.
- Lou, J., and D. J. Schwab (2000), A model of sediment resuspension and transport dynamics in southern Lake Michigan, *J. Geophys. Res.*, 105(C3), 6591–6610.
- Mehta, A. J., and E. Partheniades (1975), An investigation of the depositional properties of flocculated fine sediments, *J. Hydraul. Res.*, 12(4), 361–609.
- Otsubo, K., and K. Muraoka (1988), Critical shear stress of cohesive bottom sediment, *J. Hydraul. Eng.*, 114(10), 1241–1256.
- Parchure, T. M., and A. J. Mehta (1985), Erosion of soft cohesive sediment deposits, *J. Hydraul. Eng.*, 111(10), 1308–1326.
- Partheniades, E. (1965), Erosion and deposition of cohesive soils, *J. Hydraul. Div. Am. Soc. Civ. Eng.*, 91, 105–139.
- Robbins, J. A., and B. J. Eadie (1991), Seasonal cycling of trace elements, Cs-137, Be-7, and Pu-239+240 in Lake Michigan, *J. Geophys. Res.*, 96(C9), 17,081–17,104.
- Robbins, J. A., N. R. Morehead, B. J. Eadie, and D. N. Edgington (2003), Insights from sediment radionuclide studies in the high deposition (HiDep) area of southern Lake Michigan, paper presented at 46th Conference on Great Lake Research, 10th World Lake Conference, Int. Assoc. for Great Lake Res., Chicago, Ill.
- Schwab, D. J., J. R. Bennett, P. C. Liu, and M. A. Donelan (1984), Application of a simple numerical wave prediction model to Lake Erie, *J. Geophys. Res.*, 89(C3), 3586–3589.
- Smith, J. D., and S. R. McLean (1977), Spatially averaged flow over a wavy bed, *J. Geophys. Res.*, 82(12), 1735–1746.
- Swart, D. H. (1974), Offshore sediment transport and equilibrium beach profiles, *Publ. 131*, Delft Hydraul. Lab., Delft, Netherlands.
- Torfs, H. (1995), Erosion of mud/sand mixtures, Ph.D. thesis, Catholic Univ. of Leuven, Leuven, Belgium.
- Van Niekert, A., K. Vogel, R. Slingerland, and J. Bridge (1992), Routing of heterogeneous sediments over movable bed: Model development, *J. Hydraul. Eng.*, 118(2), 246–263.
- Vincent, C. E., and M. O. Green (1990), Field measurement of the suspended sand concentration profiles and fluxes and of the resuspension coefficient γ_0 over a rippled bed, *J. Geophys. Res.*, 95(C7), 11,591–11,601.
- Winkelman, A. G., E. R. Stabenau, and B. J. Eadie (1998), Particle size distribution and concentration of total suspended matter in southern Lake Michigan: January 28–February 10, 1998, *NOAA Tech. Memo. ERL GLERL-105*, Natl. Oceanic and Atmos. Admin., Silver Spring, Md.
- Ziegler, C. K., and B. S. Nisbet (1995), Long-term simulation of fine-grained sediment transport in large reservoir, *J. Hydraul. Eng.*, 121(11), 773–781.

N. Hawley and D. J. Schwab, NOAA Great Lakes Environmental Research Laboratory, Ann Arbor, MI 48105, USA.

C. Lee, Battelle Memorial Institute, Seattle Research Center, Seattle, WA 98109-3598, USA. (leecheeg@battelle.org)